# High-Resolution Synaptic Connectomics

**Robert E. Marc, Bryan W. Jones, Crystal Sigulinsky, James R. Anderson, and J. Scott Lauritzen**

University of Utah School of Medicine

Department of Ophthalmology

Salt Lake City, UT 84132

**Abstract** High-speed, high-resolution connectomics enables unambiguous mapping of synapses, gap junctions, adherens junctions and other forms of adjacency among neurons in complex neural systems such as brain and retina. This chapter reviews the motivations for generating complete network architectures; the technologies available for large scale network acquisition, visualization and analysis; the fusion of molecular markers with high-resolution ultrastructure; new networks and organelles discovered by ultrastructural connectomics; and new technological advances needed to expand the applications of connectomics.

2

# High-Resolution Synaptic Connectomics

## 1 Motivations for Ultrastructural Connectomics

A connectome is the complete set of cellular partners and connections for a neural region. It can be executed on the mesoscale (spatial resolution of magnetic resonance imaging or even conventional optical imaging) to map fiber networks or on the nanoscale (spatial resolution of electron imaging) to map synaptic networks. This review addresses our experience with high-resolution synaptic connectomics based on automated transmission electron microscope (ATEM) imaging.

The notion of using computational methods to accelerate ultrastructural analysis is at least three decades old (Stevens et al. 1980). Even so, computational imaging for electron microscopy did not become a mainstream strategy until recently. There were three reasons for this: slow acquisition speed, expensive storage and weak analytical scale. Film-based imaging followed by high performance digitization (Hueser 2000) or even early digital camera acquisition followed by analysis was so slow that it had no competitive advantage. Second, data storage at the resolution required for synaptic identification and quantification was prohibitively expensive, especially for NIH-funded investigators. The third reason is less obvious: No formal rationale existed to motivate large scale acquisitions.

These problems were addressed in unrelated ways. The physical acquisition problem was solved by (1) ablation sectioning and surface imaging using secondary electron imaging; and (2) true sectioning with automated primary electron imaging. Both create large digital datasets that can be navigated with computational tools and analyzed by teams. NIH and NSF initiatives to develop software for acquiring and managing these datasets were critical in making practical image volumes (e.g. Tasdizen et al. 2010; Mastronarde 2005). Further, image pyramid strategies (e.g. Google 2010) played a fundamental role in structuring applications for navigating and annotating these large volumes (Anderson et al. 2011a). The storage problem was solved by the hardware market when the price of hard drive storage dropped below 0.10 USD/gigabyte in 2009.

Previous transmission electron microscope (TEM) reconstructions were case-driven: explorations of the synaptic connectivity of specific small cells or small regions of cell networks. Sampling complete networks was not possible nor did appropriate analytical tools exist. No framework for analysis emerged that addressed neuronal population size and diversity, cell and process patterning, constraints of mapping network topologies, or specifying sampling protocols. How much data would be necessary for a real query? Nevertheless, the small scale studies that were accomplished were of exceptional quality and very high resolution (e.g. Strettoi et al. 1990; Strettoi et al. 1992). We shall return to this point, because many current efforts fall far short of the required resolution for complete connectomics analysis.

But finally, the analytical motivations for large-scale connectomics evolved in parallel with network theories of systems (van den Heuvel and Sporns 2011;

Wong et al. 2012). The proper motivation for connectomics is graph theory: the analysis of network connection patterns and how signals travel through networks (Marc et al. 2013). Formal schemas for exploring network topologies and their component motifs (i.e. stereotyped components) can scale to massive levels.

## *1.1 Network Topologies and Ground Truth*

A fundamental concept in remote sensing is *ground truth*. The reliability of any remote system of detection and classification (e.g. imaging and tracing processes and synapses) is gauged by its performance on ground truth signatures collected on-site from a validated target. The reliability of a remote platform such a TEM or scanning electron microscope (SEM) and associated algorithms in locating similar targets requires statistical definition. For biological neural networks, there is some debate about the nature of ground truth. We have made the argument that ground truth datasets for testing imaging and algorithms ought to come from neural transmission electron microscope (TEM) samples with Nyquist-compliant resolutions (Marc et al. 2013): images with resolutions superior to the structures being resolved. For synapses, gap junctions, adherens junctions, endocytosis sites, and discovery of new cell contact features, that means at least 2 nm pixel size (Anderson et al., 2011b). Previous reviews specify a 10 nm scale for connectivity analysis (Kleinfeld et al. 2011), but that is incorrect as we show below. Once sufficient numbers of connection motifs are sampled (Anderson et al. 2011a), it becomes possible to test biological variations in those motifs in development and disease. A weaker concept is the *gold standard*, which is the best reference that can be achieved under certain limitations. Arguably, once 2 nm datasets exist with appropriate instances of 0.25 nm validation (Anderson et al. 2011a; Jagadeesh et al. 2013), lower resolution gold standard sets are of limited value.

## *1.2 Graph Theory and Networks*

Graph theory provides a framework for discovering, describing, and analyzing networks of all types, including neural networks (Diestel 2005; Bollobás 1998). Neurons that integrate signals from other cells are *graph vertices* and the individual connections they form via synapses, gap junctions or other spatially discrete signaling modalities are *graph edges* (Marc et al. 2013). While classical approaches treat networks as electrical circuits, they are not loop circuits at all, but rather flow systems. Indeed, the father of classical circuitry analysis, Gustav Kirchoff, also developed many critical aspects of network graph theory for analyzing flow. More importantly, graph theory allows robust descriptions of large scale network organization. With high neuronal diversity and both dense and sparse components, it appears that biological systems-level networks like retina and brain (Perin et al. 2013) are small-world networks (Barthelemy and Amaral 1999; Barmpoutis and

Murray 2010). Such networks contain essential features of local-scale disordered Watts-Strogaz networks (1998), but in other cases show evidence of highly connected hubs, e.g. retinal AII amacrine cells (Anderson et al., 2011b). Hubs are characteristic of random systems like the World-Wide-Web (Barabási and Albert 1999), but the connectivity of retinal hubs is definitely not random. The problem of uncovering these topologies in detail falls under the field of *graph enumeration*, but the implication of high diversity was anticipated by Barmpoutis and Murray (2010) who note that in determining the range of short distance / large clustering graph distributions, that there are many graphs with short ranges but less than maximal clustering. Since there is no known evolutionary selector for maximal network clustering, this means that local network topologies cannot be inferred.

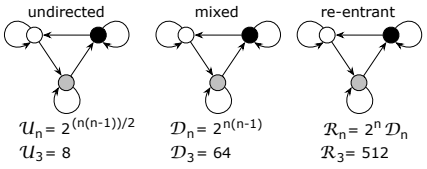


**Fig. 1** Key network enumeration relations illustrated for a simple 3-vertex cluster connected in undirected ($\mathcal{U}_n$ left), mixed ($\mathcal{D}_n$ center, directed and undirected), and reentrant ($\mathcal{R}_n$ right) configurations, where n is the number of vertices (cells).

## *1.3 Network Enumeration*

A major contribution made by graph theory to connectomics is a concrete definition of network diversity. In connectomics, we equate cells with graph vertices and their functional connections (synapses and gap junctions) with graph edges. Graph enumeration theory describes the possible network forms of any given system (Harary and Palmer 1973). Figure 1 illustrates three relations for network diversity using a simple three-vertex example. A simple undirected network (a network with bidirectional edges) with three nodes admits eight different network connections. With mixed (directed + undirected) connections, $D_s = 64$ configurations and allowing each node to possess re-entrant directed connections expands the topology space to 512 options. And this does not consider connection weight diversity. No physiological or modeling effort has proven capable of resolving even this limited diversity. In the face of real biological complexity, the challenge is beyond resolution by any inverse solution approach. In the vertebrate retina, with ≈ 70 cell classes (Marc 2010), $D_{70} = 9 \times 10^{1473}$ In the primate brain, based on known neuronal diversity and the estimated over 250 distinct brain regions, 200 of which are cortical (Van Essen et al. 2011), we can estimate that at least 1000 classes of neurons exist. So for brain, $D_{1000} = 9 \times 10^{300728}$ (Marc et al. 2012). How big is this number? The estimated number of atoms in the observable universe is $10^{80}$ and the time since the Big Bang is $4.3 \times 10^{17}$ seconds (Bennett et al. 2013). Thus even a universal computer running since the beginning of time could not parse a brain. This has distinct implications for each branch of neuroscience. Physiological mapping, even with multielectrode or optogenetics approaches (Deisseroth 2011), cannot uniquely specify correct topologies because *system transfer functions do not uniquely map onto network topologies*. This is a fundamental limita-

tion of all inverse solution approaches (Aster et al. 2005). For computing, and especially large-scale modeling (Hendrickson et al. 2012; Hay et al. 2011), sorting topologies is computationally intractable: it is the clique discovery problem, one of the best-known NP-complete problems (Karp 1972). Even simplifying concepts such as the common neighbor rule (Perin et al. 2013) do not ease the topology discovery problem. Previous modeling efforts in simple invertebrate networks (Prinz et al. 2004) have been argued as evidence that morphologic topology may be neither stable nor definitive, and that different individual network weights in *each different animal* may lead to similar network performance. In this view, connectomics is not a viable effort. Morgan and Lichtman (2013) give a strong defense of connectomics on this point, but it can be further argued that the high diversity of modeling solutions obtained by Prinz et al. (Prinz et al. 2004) means that network topology and synaptic weights *must both* be demonstrably constrained to develop a functioning system of repeating units known to underlie vertebrate brain and retinal organization (Marc et al. 2013). Ultimately, due to the massive diversity of neuronal classes, classical TEM sampling has been unable to completely specify any outflow module in the retina, much less any other complex brain region. However, discrete, complete topologies can be discovered by connectomics.

# 2 Technologies

## *2.1 Biological Motivations for High Resolution Ultrastructure*

Complete connectomics requires being able to trace all neurogliovascular associations of brain and retina, not simply detecting the easiest or most common motifs. Among sets of neurons this is includes connection types and *non-connections*. The occurrence of a connection between a pair of cells (an edge between vertices) is a nominal proof of its typological existence, and its expected density can be computed from spatial dimensions of the chosen canonical field. Evidence of a non-connection, however, is statistical, as one can only assert the absence of a connection over a sampled field, compared to realized connections. There are two types of non-connections: those arising from (1) spatial separation where two kinds of cells never touch and, more importantly, (2) *touches*: contacts that form no connections despite opportunity. The latter implies deterministic rather than strictly probabilistic events in network assembly. There are five types of cell adjacency: touches, adherens, synapses + adherens, gap junctions + adherens, and synapses + gap junctions + adherens. Synapses and gap junctions never appear without nearby adherens complexes (Fig. 2).

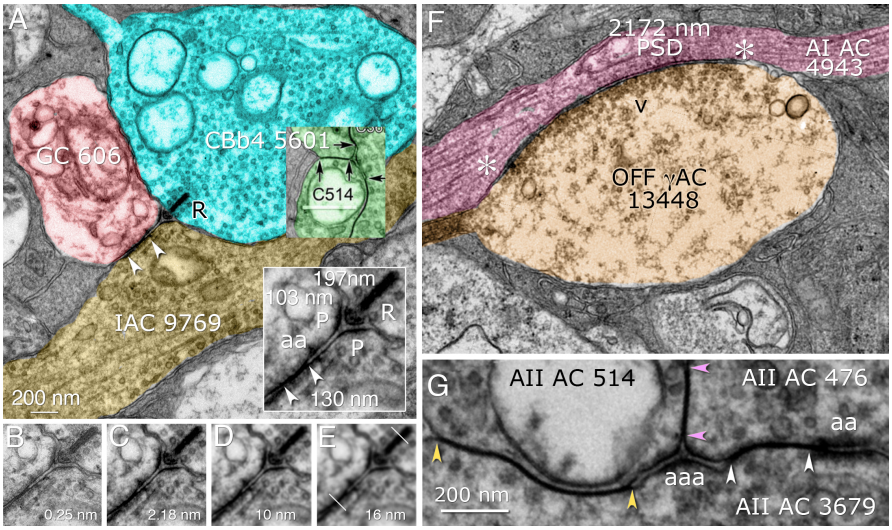


**Fig. 2.** Cell associations imaged with high-resolution ATEM. A. A complex synapse involving excitatory ribbon drive from a glutamatergic bipolar cell (CBb4 5601) targeting a ganglion cell (GC 606) and a GABAergic amacrine cell (IAC 9769), and direct gap junction coupling between cells 606 and 9769. The insert marks a presynaptic ribbon (R) 197 nm long, a postsynaptic density (P) in ganglion cell 606 (103 nm) and amacrine cell 9769, the gap junction (bracket by arrowheads) between cells 606 and 9769, and a focal adherens junction (aa). B. The inset region re-imaged by goniometric tilt TEM with a resolution of 0.25 nm/pixel and a tilt of 5° from planar. C. The primary image captured by ATEM with a resolution of 2.18 nm/pixel. D. A simulated 10 nm/pixel resolution capture using a boxcar blur. E. A simulated 16 nm/pixel resolution capture using a boxcar blur. The length and nominal position of scan paths used to profile the synaptic ribbon and gap junction are shown as lines. F. A giant conventional form inhibitory synapse between an OFF cone pathway GABAergic amacrine cell (γAC) 13488 and a rod pathway AI AC 4943. G. Three gap junctions between three different AII ACs ( 476, 514, 3679) bracketed by 2-cell (aa) and 3-cell (aaa) adherens complexes. All data from the open-access RC1 connectome.

The task of completely specifying the network associations of a cell depends on the reliability of discriminating contact types in a full 3D setting, which includes both ideal transverse and non-ideal oblique sections through synapses, gap junctions, adherens junctions and other para-membrane specializations. Bluntly, scanning electron microscope (SEM) imaging has never been competitive with TEM imaging for connectivity analysis. Indeed, after a half-century of technical development, SEM still cannot provide the resolution of even the earliest TEM studies for synaptic analysis (Cohen 1965), and has never been the platform of choice. The question at hand is whether connectivity analysis by new SEM imaging is as reliable or complete as ATEM analysis. Part of the argument for SEM imaging is that it may visualize synapses adequately, even if not optimally.

While some presynaptic and postsynaptic features are supraoptical (>200 nm), most are not. Figure 2 shows a complex glutamate synapse in rabbit retina between an ON cone bipolar cell and two targets at a classical bipolar cell dyad. While the presynaptic ribbon is just at the limit of optical resolution, the postsynaptic densities (PSDs) of the ganglion and amacrine cell targets are both far smaller, on the order of 100 nm. Similarly, the entire gap junction is suboptical.

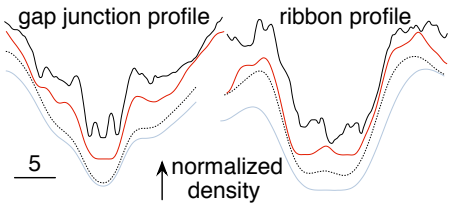


**Fig. 3** Pixel density scans of a gap junction and synaptic ribbon shown in Fig. 2 at varying resolutions in nm/pixel: 0.25 (black), 2.18 (dotted), 10 (red), 16 (grey). Imaging at 0.25 nm reveals the characteristic profiles of both structures. Resolutions used for connectomics lose details but 2 nm resolution retains enough high-frequency components to distinguish them.

Definitive gap junction mapping requires picoscale imaging (Fig. 3). The spot adherens (Fig. 2A) is less than 30 nm in extent. This is non-trivial, as adherens junctions likely mediate protein delivery to and turnover of gap junctions (Lynn et al. 2012; Li et al. 2008) and synaptic junctions (Mizoguchi et al. 2002; Benson and Huntley 2012; Ogita et al. 2010). Identifying contacts of these dimensions requires ground truth quality imagery, not 10-16 nm scale imaging typical of SEM data. Figures 2A-E show the progressive degradation in image quality associated with 2 nm ATEM imaging (Fig. 2C), nominal 10 nm imaging (e.g. Kleinfeld et al. 2011) and 16 nm imaging characteristic of much published serial bloc-face (SBF) SEM imaging. Indeed the degradation at 16 nm is so marked that no validated gap junctions or bipolar cell synapses have yet been illustrated as part of any SBF connectomics analysis (Briggman and Denk 2006; Briggman et al. 2011; Helmstaedter et al. 2013). In contrast, 2 nm resolution ATEM easily detects all synapses and gap junctions, as well as validating non-contacts (Marc et al. 2013; Lauritzen et al. 2012; Marc et al. 2012; Anderson et al. 2009). The quality of these images is compared by density scans of critical features such as ribbons and gap junctions (Fig. 3), both of which are easily confused with PSDs and adherens junctions in automated detection systems, but are readily marked correctly by human annotators. Importantly, the severe blurring of gap junctions, synaptic ribbons and PSDs at SBF scales makes these structures effectively indistinguishable. While the ability of ATEM to track these small contacts is critical to complete analysis, so too is ongoing validation by re-imaging at ground truth level. We have found that selective homocellular gap junctions coupling cone bipolar cells into class-specific sheets (Lauritzen et al. 2013) are extremely small (60-90 nm), formed by small processes of similar diameter. Validating these and similar contacts requires a ground truth resolution of smaller than half the size of the smallest structure that serves as a discriminator. In this case the discriminant would be the gap between the outer leaflets of the coupled membranes. In retinal gap junctions, especially those involving amacrine cells, the feature would be the 1.8 nm gap (Marc et al. 1988). If we model that gap as a three segment trapezoid profile, each segment would have to be 0.6 nm and the sampling rate would need to be 0.3 nm/pixel, which is why we have chosen 0.25 nm as our ground truth resolution. We have discovered that, even with 2 nm ATEM resolution, gap junctions of less than 90 nm in planar extent and oblique tilt of ≥ 45° cannot be discriminated from similar sized adherens junctions. Indeed our success rate is exactly 50%. Thus, as these specific contacts are identified, it is essential that many be validated by re-imaging

at ground truth resolution. So far, only ATEM methods have proven capable of re-imaging ultrastructural features (Anderson et al. 2011b).

## *2.2 Samples, Ablation Sectioning, True sectioning and Imaging*

Conventional fixation with mixed aldehydes, osmium en bloc staining and optional *en bloc* uranyl acetate for electron imaging is optimal for ATEM. We use a Karnovsky's variant with light osmication. We do not use ferrocyanide staining as iron atoms cannot be removed for post-embedding immunocytochemistry, which is one of our major tools. In contrast, SEM methods require substantial enhancement of membranes for tracking and synapse identification and use of osmium-thiocarbohydrazide-osmium and ferrocyanide is common. Since these metallization approaches cannot be reversed, SBF / FIB imaging is incompatible with molecular markers.

There are three sectioning technologies under exploration. Ablation methods use physical sectioning with an automated microtome, such as *in vacuo* SBF sectioning (Briggman and Denk, 2006; Denk and Horstmann, 2004) or surface ablation via in vacuo field ion beam (FIB) milling (Knott et al. 2008; Morales et al. 2013), followed by scanning electron microscope (SEM) or scanning TEM (STEM) imaging of secondary electrons (surface-backscattered electrons). Ablation techniques require very thin sectioning steps (Boergens and Denk 2013) as secondary electrons are surface reflections of the sample and do not penetrate deeply. This surface imaging approach leads to excellent binarization of membrane images for tracing, but is quite sensitive to skips in data. It also limits resolution because electron beams can only be reduced to nanometer scale widths, and acquisition times can be quite long for large sample fields. Ablation methods are also incompatible with *en bloc* molecular markers for proteins and small molecules, so far. However, these are superb methods for wide-field connectomics: getting the broad-brush view of connectivity which high-resolution connectomics can then refine.

Manual ultramicrotomy using existing platforms remains a reasonable alternative to specialized ablation systems (Bourne and Harris 2011; Anderson et al. 2009). Microtomists can produce hundreds to thousands of serial sections with minor errors and much less time than required for TEM acquisition. Sections are placed on monomolecular films, followed by conventional metal staining and ATEM (Anderson et al. 2011b; Anderson et al. 2009). Primary electron projection images of sections 50-70 nm thick can be used as 2D pages in a 3D volume, or assembled as true 3D datasets. Because the data are projection images, they can be further refined by goniometric re-imaging. In addition, intercalated thin sections are placed on slides for computational molecular phenotyping every 20-30 TEM sections, permitting the insertion of molecular data into the connectome (Fig. 4). Finally robotic sectioning onto Kapton® films (Kleinfeld et al., 2011) is a new but not readily usable option. Hopefully that technology will advance to the point of enabling more efficient use of existing TEMs by using electron-transparent films.

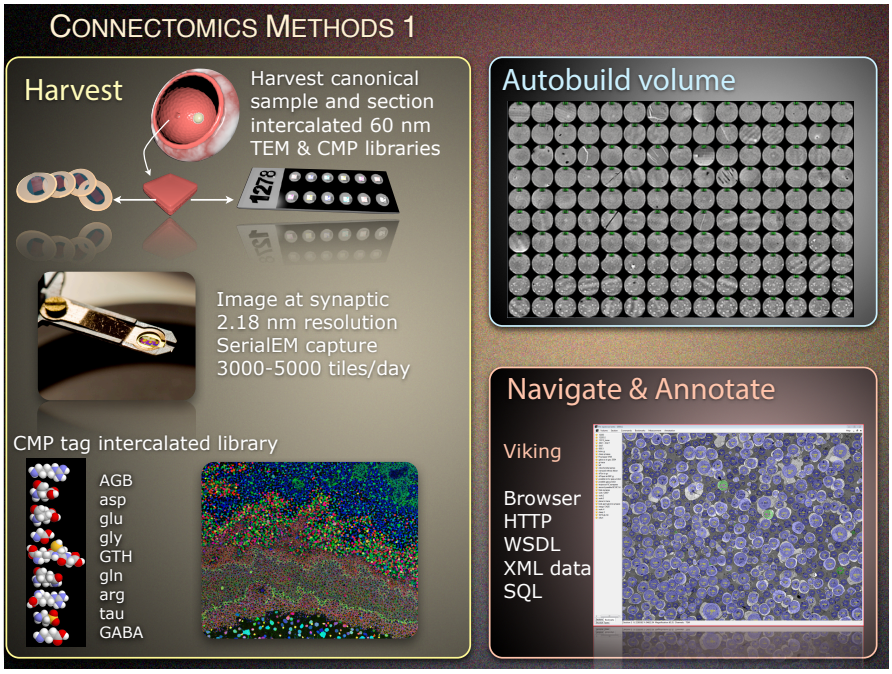


**Fig. 4** Workflow for building connectomics volumes. Samples containing a canonical field are fixed for TEM, embedded and serially sectioned onto TEM grids with intercalated CMP sections placed on array slides. Fields are imaged at synaptic resolution and captured using SerialEM automation. Slides are probed for an array of small molecules that give complete cellular coverage and high levels of classification. About 1000 TEM image tiles are mosaicked into single image slices and slices registered into aligned volumes that can be visualized in the Viking navigation and annotation environment.

## *2.3 Molecular markers and Classification*

The synaptic resolution of electron optical imaging comes at a significant price: the restricted ability to use typical macromolecular molecular markers to classify cells. Neuronal classification has been based on Golgi impregnation or dye marking of cells, and more recently, by expression of genetic markers. All these approaches led to consistent estimates of cell diversity in the retina (MacNeil et al. 2004; Rockhill et al. 2002; MacNeil et al. 1999). Morphologic features have not proven useful for extending these classifications (e.g. cell diameters, Scholl rings, fractal analysis of dendritic arbors). An alternative approach, computational molecular phenotyping (CMP) developed by Marc et al. (Marc and Jones 2002; Marc and Cameron 2001; Marc et al. 1998; Kalloniatis et al. 1996; Marc et al. 1995) allows fusions of structural and molecular profiling using pattern recognition yielding neuron classification equivalent to prior anatomic studies. Based on formal

theories of unsupervised multidimensional classification derived in remote sensing (Cover and Hart 1967; MacQueen 1967) and clustering algorithms such as the K-means and isodata methods, CMP led to robust classifications, but achieved them in single retinas instead of hundreds (Marc and Jones 2002; Marc and Cameron 2001; Marc et al. 1998; Kalloniatis et al. 1996; Marc et al. 1995). CMP is compatible with ATEM (Marc and Liu 2000). The superiority of multivariate small molecule signatures over other TEM visualization methods also comes from its coverage. While there are over 60-70 classes of cells in mammalian retina (neurons, glia, microglia, vascular cells), and some are identifiable with antibodies targeting macromolecules, most are not TEM-compliant and such univariate markers have very narrow coverage. Even with a theoretical experiment involving 8 macromolecular tags, far less than 10% fraction of any neural system is classified. Conversely, small molecule tags like glutamic acid embedded in a CMP schema quantitatively discriminate many classes of cells (Marc and Jones 2002; Marc and Cameron 2001; Marc et al. 1998; Kalloniatis et al. 1996; Marc et al. 1995; Marc et al. 1990; Chua et al. 2013). CMP places multiple signals in every cell in a TEM dataset, so that even if a biologically ultimate class cannot be extracted for each, at least a very well defined superclass cohort can be specified.

## *2.4 Computational TEM: Fast High-Resolution Acquisition*

Each slice of a connectome volume is composed of >1000 image tiles and can contain 100s to 1000s of slices (Fig. 4,5). This means that capture needs to be high speed and automated. For our version of ATEM, individual grids are loaded manually into a goniometric holder and imaged at ≈ 5000x magnification in a grid pattern with roughly 12% edge overlap using a JEOL JEM 1400 TEM and a Gatan Ultrascan phosphorimaging camera (Anderson et al. 2011b; Tasdizen et al. 2010; Anderson et al. 2010; Anderson et al. 2009). In the rabbit retinal connectome RC1 (Anderson et al., 2011b) each image slice (the digital transform of a physical section) contains a canonical field 0.243 mm diameter and, at a resolution of 2.18 nm/pixel, and requires 950-1100 individual images. Stage motion, focus and image capture are achieved by SerialEM, developed by David Mastronarde at the University of Colorado, Boulder (Mastronarde 2005). Modifications to SerialEM also allow sections to be pre-heated in a wide beam for film stabilization and complex patterns of image acquisition.

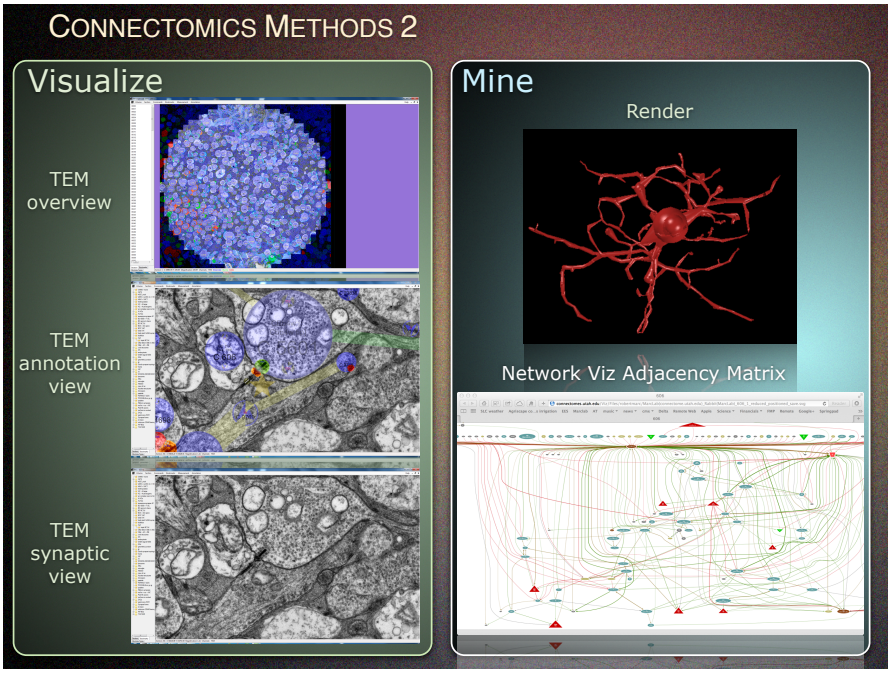


**Fig. 5** Workflow elements for analyzing high-resolution connectomics volumes. Volumes are navigated at any desired resolution and annotated using the Viking navigator and annotation client. Individual synaptic fields can be rendered for image publication within Viking. Viking disk annotations contain all the information necessary to build accurate 3D cell volumes and visualize complete networks. Vikingplot is a MatLab® application that queries the SQL database to provide 3D rendering of individual cells or even all cells in the volume as individual images, stereo images or fly-through movies. Network Viz is a graphing client that visualizes adjacency matrices of connected cells in a volume and allows queries of Viking.

## *2.5 Image Volume Visualization and Annotation*

Conventional imaging tools are incapable of visualizing datasets as large as a connectome, much less navigating them in a structured way. New tools are required (Fiala 2005; Jeong et al. 2010; Anderson et al. 2011a; Helmstaedter et al. 2008). By using image pyramid sets (Mikula et al. 2007; Anderson et al. 2011a), web-applications can readily view, transform and annotate connectomes. Anderson and colleagues (2011a) have developed Viking to address these needs. Viking has a three-tiered architecture in which tier 3 viewer and analysis clients use HTTP to communicate with Tier 2 image and WSDL-compliant web servers which in turn query the Tier 1 image library and populate annotations in a Tier-1 SQL database (Fig. 6). Viking operates by HTTP and supports concurrent multi-user, collaborative annotation. By demarcating viewing and analysis from data collection and hosting this architecture allows independent tier specialization. Most importantly,

it is capable of applying image transformations in real-time for high-speed visualization. Human operators use disc-based annotation, centering an appropriately sized disc in every neural profile which Viking links into a network of graphs (Fig. 5,6), 3D navigational skeletons, databases and 3D renderings in multiple formats at 2 nm or better resolution. Presynaptic ribbons, patterned densities, vesicle clouds, postsynaptic densities, gap junctions, adherens junctions are all characterized by their connectome physical locations, dimensions and parent structures, allowing the assembly of formal adjacency matrices.

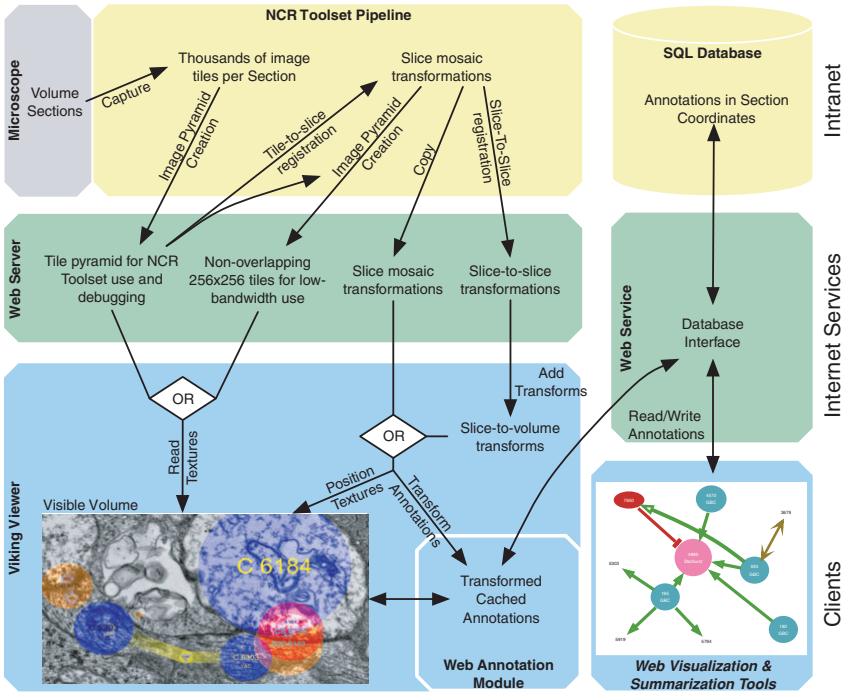


**Fig. 6** Overview of the integrated image transform-Viking functions. Viking is a scalable annotation environment, based on a three-tier architecture. Tier 1 processes the TEM image data and maintains the SQL database maintenance in a secure environment isolated from the Internet. Tier 2 servers form the web services definition language (WSDL) interface whereby transfers images, transforms, and annotations are negotiated between clients and Tier 1. Tier 3 is composed of our Viking viewing/annotation client and Viz analytics tools. Method calls between layers are stateless and the tiered architecture permits independent tier modification. From Anderson et al. (2011a) by permission of the authors.

## *2.6 Analysis: Automated vs Authenticated Synapse Tracing*

Retinal connectome RC1 is a connectome in an advanced state of annotation with ≈ 900,000 embedded annotations. RC1 is an open-data resource. The entire volume, all of its imagery and all of its annotations are publicly available (Anderson

et al. 2011b; Lauritzen et al. 2012) and any portion of it may be reproduced under a Creative Commons Attribution-NonCommercial 4.0 International License. No imagery or data from RC1 can be restricted by publication copyright. Even though it contains over 300 bipolar cells (BCs), 300 Müller cells (MCs), 39 AII ACs, over 100 ACs, and 20 ganglion cells (GCs) and includes a full set of small molecule markers for classification, it is far from complete. A spectrum of solutions has been proposed to complete the annotation set, ranging from automated detection schemas (Jagadeesh et al. 2013) to high density crowd sourcing (Helmstaedter et al. 2013; Briggman et al. 2011). We were one of the earliest proponents of crowd-sourcing (Anderson et al. 2009) and have retreated from that position somewhat to advocate an executive annotator + team format. One of the major problems of automated and crowd-sourcing approaches is resolving contact error detection and correction. The ease with which both software and novice annotators confuse oblique synapses, adherens junctions and gap junctions demands a ready correction schema. In theory, any automated system must be tested against a ground truth dataset (Jagadeesh et al. 2013), but no one has proven that any automated system can discriminate these components. We have three practical solutions. First, errors in identification create violations of well-known connectivity rules: e.g., retinal ganglion cells are always postsynaptic, bipolar cells are never presynaptic to each other, rod bipolar cells form no gap junctions, OFF cone bipolar cells form no heterocellular gap junctions (so far), ON bipolar cells are not coupled to ganglion cells. Any such aberrant contacts in a network build can be readily flagged by database queries for reconciliation by an experienced analyst. Second, albeit slower, goniometric re-imaging can validate or reject unusual contacts. Third, our annotation training is intense. All new annotators serve an apprenticeship directed by a proven low-error annotator. Finally, as the entire volume is open-access, any error can be corrected by later annotators.

## 3 Discovery

A key objective in developing high-resolution connectomics technologies arose directly from our own prior work identifying a broad array of complex nested amacrine cell networks that have yet to be explained in any retina (Marc and Liu 2000). Analysis of RC1 has subsequently discovered new motifs and synaptic / coupling architectures. Here we present a selection of those discoveries.

### *3.1 Novel Networks Refactor the Retinal Inner Plexiform Layer*

In the process of tracing rod-cone pathways, we noted two abundant suboptical architectures that changed the expected patterning of signals in the mammalian inner plexiform layer: nanoscale ON bipolar cell axonal synaptic ribbons (Fig. 7)

and nanoscale OFF bipolar cells with descending axonal processes. By annotating all bipolar cells in RC1 (≈ 300), we defined rod bipolar cells and two superclasses of cone bipolar cells: ON (CBb cells), and OFF (CBa). CBa and CBb cells are fully distinguished by three features: (1) CBa cells terminate primarily in sublayer a with fine processes into the upper sublayer b, while CBb cells terminate primarily in sublayer b with axonal outputs in sublayer a; (2) CBa cells are both presynaptic and postsynaptic to AII amacrine cells, while CBb cells are instead coupled to AII amacrine cells by large gap junctions; and (3) CBa cells have a strong primary glutamate signature while CBb cells have a mixed glutamate-glycine signature due to coupling with glycinergic AII amacrine cells. But complete annotation allows further refinement of cone bipolar cells into ultimate classes including 6 OFF (CBa1, CBa1w, CBa1-2i, CBa2, CBa2w; CBab2) and 7 ON (CBb3, CBb3-4i, CBb4w, CBb4-5i, CBb5w, CBb6w, and CBb7w) cone bipolar cells, where the number indicates a progressively more proximal stratification, i denotes an interlaced axonal pattern, and w denotes wide field axonal arbors. In the process of this complete annotation we found abundant suboptical (<100 nm) synaptic ribbons and vesicle assemblies in the axons of CBb cells (Anderson et al. 2011b). Upon reconstruction, we showed that these represented a novel ON pathway input to the OFF layer of the inner plexiform layer (Lauritzen et al., 2012), verifying the optical immunocytochemical visualization of synaptic ribbon proteins by Dumitrescu et al. (2009) and Hoshi et al. (2009). High-resolution connectomics then enabled a complete connectivity analysis. Connectomics of RC1 (Lauritzen et al. 2012) showed that: (1) 36% of CBb cells form OFF layer axonal ribbons (Fig. 7, 8); (2) all classes of CBb cells contribute to this motif, targeting ON ganglion cells that arborize in the OFF sublayer, e.g. intrinsically photosensitive ganglion cells and bistratified diving ganglion cells; and (3) specific glycinergic and GABAergic amacrine cells engaged in ON → OFF crossover signaling were targeted. These data completely revise the notion that amacrine cell and ganglion cell stratification patterns alone control access to ON and OFF inputs. More detailed discussion of the implications of this motif are available in Marc et al. (2013). No SEM schema has detected these motifs.

Similarly, the ON sublayer of the inner plexiform layer is not a pure ON signal domain. Lauritzen et al. recently discovered that the upper half of the ON layer contains significant numbers of ribbon outputs arising from fine descending processes of OFF cone BCs, forming a large band of commingled CBa and CBb cell inputs in IPL sublayers 3-5. These processes are usually <100 nm in dimeter and synaptically target amacrine cells. Once again, these are processes that have been missed by lower resolution technologies such as SBF SEM (Helmstaedter et al. 2013). This branching permits intermixed ON class and OFF class processes to target single glycinergic and GABAergic amacrine cells, generating ON-OFF functions. These new sets of bipolar cells are termed CBab cells. They are, nevertheless, classical OFF cone BCs as their primary arbors are in the OFF layer; they are coupled to other OFF bipolar cells in homocellular arrays; they are presynaptic and postsynaptic to AII amacrine cell lobules; and they are glycine-negative. The diversity of contacts is as complex as for axonal ribbons. CBab cells provide direct ribbon drive to at least one ganglion cell class in the ON layer and synapse onto amacrine cells throughout the nominal ON layer of the inner plexiform layer, cre-

ating ON-OFF amacrine cells that likely drive all ON bipolar cell surrounds. Thus CBab cells form specific ON-OFF subnetworks that could not otherwise be constructed. These unpredicted network topologies may underly widespread ON-OFF signaling in the retina.

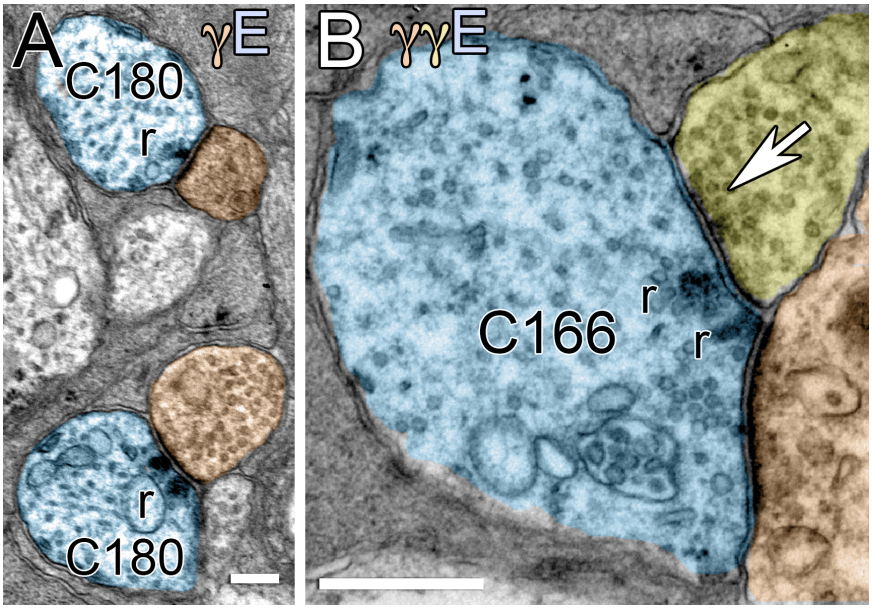


**Fig. 7** Axonal ribbons made by ON bipolar cells in RC1. (A) Axonal ribbons (r) at mid-axon (blue) from ON cone bipolar cell 180 to AC targets (orange) in the OFF sublayer. Cell 180 splits high in the OFF sublayer and makes axonal ribbons immediately after the split. (B) Axonal ribbons from ON cone bipolar cell 166 onto two different targets (orange, yellow), one of which makes a feedback synapse (arrow). Note the distinctive postsynaptic densities in the targets. Scales, 500 nm. γ GABA, E glutamate. Recomposed from Anderson et al. (2011b) by permission of the authors.

These new findings suggest a revision of the traditional view of inner plexiform layer organization in the mammalian retina. First, there is no pure OFF layer as it is completely patterned with ON inputs from axonal ribbons. Second, the central regions of the inner plexiform layer is composed of mixed ON and OFF cone bipolar cells whose surrounds are ON-OFF, since they are driven by GABAergic and glycinergic amacrine cells that collect inputs from both ON CBb and OFF CBab cells. Finally, the "pure" ON zone is restricted to a thin layer of rod bipolar cells and wide field ON cone bipolar cells. This refactoring implies that multistratified amacrine and ganglion cells cannot be assumed to be ON-OFF in polarity, and that monostratified amacrine and ganglion cells cannot be assumed to be pure OFF or pure ON. Complete connectivity maps must be derived for every cell class.

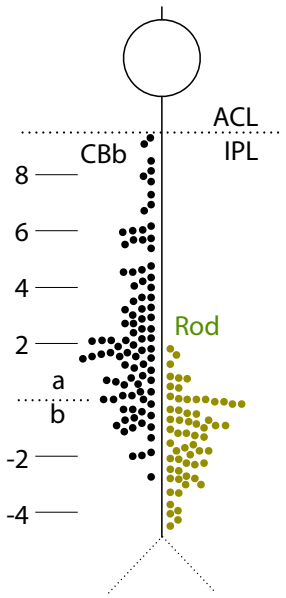


**Fig. 8** Axonal ribbons. The distribution of 160 axonal ribbons in 54 ON cone bipolar cells and 63 of the highest ribbons in 63 of 104 rod bipolar cells in connectome RC1. Ribbon positions are measured relative to the sublayer a/b border, defined as the proximal face of the nearest AII AC lobule. ON cone bipolar cell axonal ribbons are distributed throughout sublayer a. Rod bipolar cell axonal ribbons are excluded from 80% of sublayer a. From Lauritzen et al. (2012), by permission.

## *3.2 Bipolar Cell Coupling Arrays*

Homocellular coupling between neurons such as horizontal cells or AII amacrine cells, and heterocellular coupling between ON cone bipolar cells and AII amacrine cells (using the notation CBb::AII) has long been known (Kolb and Famiglietti 1974a; Kolb and Famiglietti 1974b; Famiglietti and Kolb 1975; Kolb 1977; Raviola and Gilula 1975). These gap junctions are often large and/or abundant. However, the neural retina contains numerous classes of highly branched cells such as cone bipolar cells, and tracing their processes has heretofore proven challenging. Even markers selective for single classes do not allow tracing of suboptical processes, nor visualization of suboptical gap junctions (Lee et al. 2011). By tracing every class of cone bipolar cell, we discovered extensive axonal coupling within but not between CBa and CBb superclasses (Lauritzen et al. 2013). Within each superclass, both in-class (homocellular, e.g. CBb4w::CBb4w) coupling sheets and cross-class (heterocellular, e.g. CBb3::CBb3-4i::CBb4w) coupling tiers exist. Cross-class coupling occurs between neighboring CBb pairs because their stratifications overlap vertically and laterally. As many CBb cells appear to express Cx36 (Han and Massey 2005), this may explain in-class and cross-class coupling. These networks are sparse: five CBb5w bipolar cells (Fig. 9) coupled at five loci represents a cellular volume spanning >39,000 distinct high-resolution images. The probability of finding any of these gap junctions randomly by TEM is far less than 1 in 10,000 image sessions. Without 3D tracing it is impossible define the cell of origin. Only through connectomics can we find biological relationships that are sparse, yet pervasive. Further, the largest dimension of the gap junction at one locus between cells is ≈ 140 nm, far below the limit of optical imaging. Tiered coupling in the ON pathway (e.g. CBb3::CBb4::CBb5) excludes CBa or rod bipolar cells. The physiological implications are yet unclear. It is possible that cone bipolar cells use coupling to smooth signaling transitions across classes with different dynamic ranges, or smooth inhibition across patches of cells. CBa::CBa coupling is also extensive. Coupling may play a role in the development of cone bipolar cell terminal tiling.

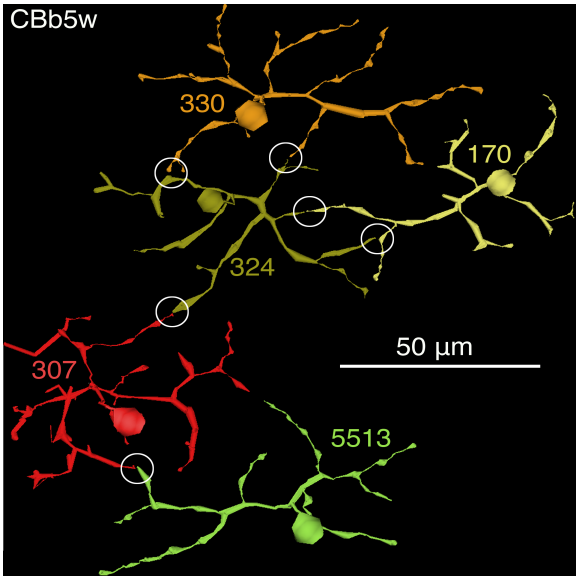


**Fig. 9** Homocellular bipolar cell coupling. A coupled sheet of CBb5w cells viewed in the XY plane (the retinal image plane). Each color denotes a different cell of the same class and circles mark points of coupling. VikingPlot rendering of data from the open-access connectome RC1. Lauritzen, unpublished.

### *3.3 Advanced Networks: Rod-Cone Suppression, Nested Feedback*

Inhibitory networks dominate the retina. Over 90% of the mass of the vertebrate inner plexiform layer is made of GABAergic neurons. The most common synapses are amacrine cell synapses. The most common motifs are amacrine-to-amacrine synapses (Marc and Liu 2000). Yet there are no models that require or explain this attribute. By mining the *complete* connectivities of certain cells, we have been able to extract key architectures such as decision networks. We have also been able to define participants in serial amacrine cell motifs, some of which represent nested feedback and feedforward architectures introduced by Marc and Liu (2000). These networks could not have been identified by statistical methods.

Inhibitory decision networks are the essential components of sensory "trigger features," such as motion. Similar decision processes have been implicated in rod-cone interactions by psychophysical analyses (Stabell and Stabell 1998, 2002; Trezona 1970, 1973; Thomas and Buck 2006; Brill 1990; Frumkes and Eysteinsson 1988; Goldberg et al. 1983; Lange et al. 1997; Buck 2004). Such interactions are surprisingly fast and often involve small spatial fields (Thomas and Buck 2006; Buck et al. 1984; Buck 1997, 2004). Rods can also induce a variety of chromatic effects in cone pathways (Stabell and Stabell 1998). What are the pathways underlying these operations?

Connectomics analysis of RC1 shows that at least eight unique suppression motifs exist between rod bipolar cells and cone bipolar cells (Marc et al. 2013), and that these are mediated by several different sets of amacrine cells (Fig. 10). Cone pathway suppression of rod pathways is mediated by five distinct motifs initiated in all cone bipolar cell classes. Rod bipolar cells receive inhibition by ON

cone bipolar cells via motifs C1 and C2; and inhibition by OFF cone bipolar cells via motifs C3, C4 and C5. Rod pathway suppression of cone pathways is mediated by three distinct motifs targeting all cone bipolar cell classes. ON cone bipolar cells receive powerful suppression via motifs R1 and R3, while motif R2 suppresses OFF cone bipolar cells. These motifs are consistent with a range of psychophysical results and show that there is complete suppressive crossover between all cone bipolar cells and rod bipolar cells. This was not known prior to high-resolution connectomics.

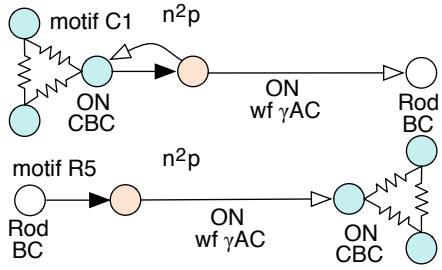


**Fig.** Two of the eight rod-cone decision networks discovered in open-access connectome RC1. In motif C1, couple patches of ON cone bipolar cells (ON CBC) drive wide-field feedback / feedforward ON GABAergic amacrine cells (ON wf γAC) that inhibit rod BCs. In motif R5, rod BCs drive feedforward ON wf γACs that inhibit ON CBCs..

While amacrine cell serial synapses have been described for over half a century, their role has been completely unknown, even though they are the most common synapses in the inner plexiform layer (Marc and Liu 2000). Using limited series of TEM sections, Marc and Liu (2000), using limited series of TEM sections, showed that nested feedback was a dominant motif in the vertebrate inner plexiform layer, but could not identify all the partners. Using comprehensive connectomics, it has now been possible to show that all cone bipolar cell feedback amacrine cells engaged in a variety of nested topologies. Indeed, there is no simple first-order feedback. There are a large number of possible nesting topologies and several have been documents. One example is multichannel nesting where a pure feedforward GABAergic interstitial amacrine cell collects signals from several classes of ON cone bipolar cells (IAC, cell 9769, Figure 11) and is both presynaptic and postsynaptic to a different wide-field GABAergic amacrine cell (wf AC, cell 24381, Figure 11)) that is itself part of a more different ON cone bipolar cell feedback network. This reciprocal relationship simultaneously creates both nested feedback to bipolar cells through the CBb > IAC >i fw AC >i CBb, and nested feedforward to target ganglion cells CBb > wf AC >i IAC >i GC.

The advantage of nesting low gain inhibition (i.e. feedback networks inhibiting themselves as well as their targets) is that it is the *simplest form of network tuning possible*. The concept is realized in many forms in modern electronics, such as nested transconductance amplifiers, where the depth, polarity and strength of nesting shapes the frequency response of the network (Xie et al. 1999). Marc and Liu (2000) described how such a network could improve the bandpass of bipolar cell output (Figure 12) by increasing both the system corner frequency and bandwidth. Of course this is only a simple linear systems analysis, and in spiking networks, these attributes can be even more potent, forming into critical timing networks.

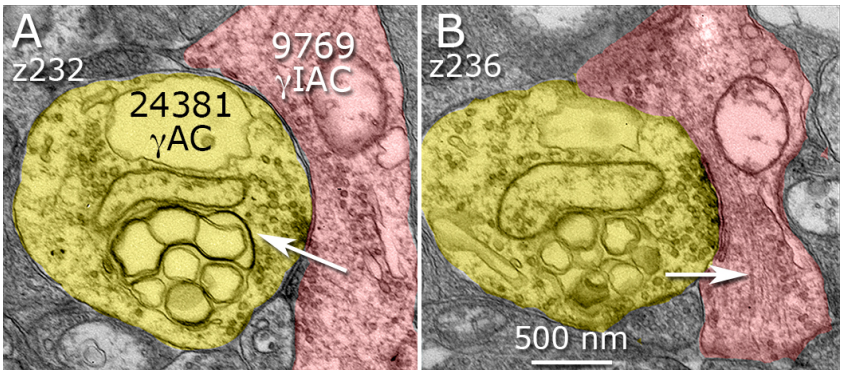


**Fig. 11** Nested inhibition between different classes of amacrine cells. **A**. Wide-field GABAergic feedback amacrine cell 24381 is postsynaptic to GABAergic feedforward interstitial amacrine cell 9769 (arrow) at slice z232 in retinal connectome RC1. **B**. Cell 24381 is presynaptic to cell 9769 (arrow) at slice z236.

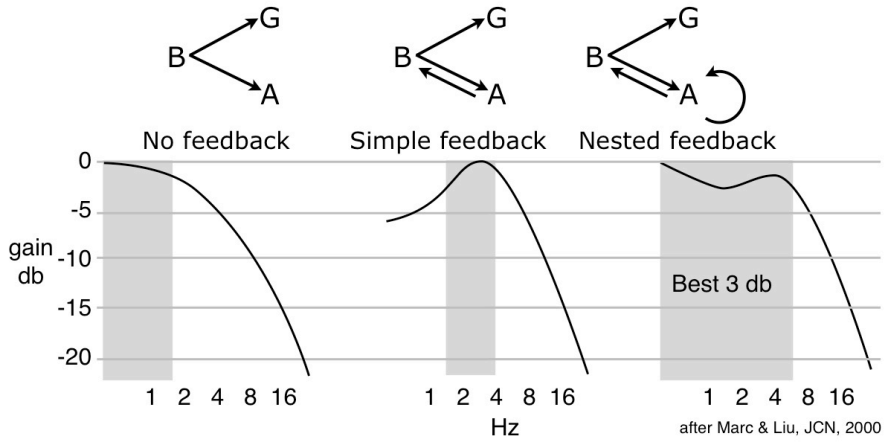


**Fig. 12** The effect of nested inhibition on network properties as modeled by Marc and Liu (2000). The top row illustrates the topologies of networks among bipolar (B), amacrine (A) and ganglion cells (G) with no feedback, simple first-order feedback, or nested feedback. The bottom panels illustrate the frequency response properties (ordinate in db, decibels; abscissa in Hz, cycles per second) of bipolar cell output under the three conditions. Simple feedback classically increases the corner frequency from a simple rolloff (left) to a bandpass form (middle) at the expense of low frequency rolloff. Nested feedback attenuates the rolloff and essentially spreads the bandwidth (the best 3 db range) 2-3 fold.

## *3.4 New Structures*

Since the 1960s, ultrastructural analysis of brain and retina has depended on known morphologies: chemical synapses, gap junctions and adherens junctions. In analyzing connectome RC1, especially during complete neuronal mapping, new

contact architectures were discovered (Marc et al. 2013). Their full description is outside the scope of this review, but they are examples of the power of high-resolution 3D mapping.

*Cistern contacts* were first found between ON cone bipolar cell axons and amacrine cells (Anderson et al. 2011b; Lauritzen et al. 2012). They are characterized by post-cistern density that resembles a conventional postsynaptic density (PSD). The pre-cistern structure is smooth endoplasmic reticulum (SER) loop.

*Rough endoplasmic reticulum* (RER) contacts resemble cistern contacts and appear initiated by amacrine cells in most cases. Two or flattened SER cisterns on the pre-RER side are capped by a loop of RER, and the opposing processing displays a PSD similar to a conventional excitatory synapse. RER contacts can originate both in and far from neuronal somas, and we envision the contact using a signaling peptide requiring local synthesis.

*Bipolar cell conventional* (BCC) synapses are large synapses found in bipolar cells that resemble conventional brain glutamate synapses. First described in human retinas (Allen 1969), they have been completely ignored since. Normally, bipolar cells are defined as cells that use synaptic ribbon complexes for glutamate signaling. However cone bipolar cells (not rod bipolar cells) can also display synapses without synaptic ribbons and target cells that use very large PSDs. Interestingly, some BCC synapses target only specific cells (including directionally selective ganglion cells). We hypothesize that BCC synapses drive transient events while ribbon synapses drive sustained signaling.

*Keyholes* are unusual and rare structures formed mostly by CBb3 ON bipolar cells and CBa2 OFF bipolar cells. Keyholes are loops formed by bipolar cell axon terminal tendrils recurving to contact the parent terminal with a gap junction. In the process they surround fine amacrine cell processes, some as as small as 30 nm. We do not know if keyholes are functional. If so, they may act as low-gain ephaptic signaling sites.

*Plaques* are large, dense, osmiophilic cisterns formed at the plasmalemma by ganglion cells primarily in their somas or proximal dendrites, adjacent to Müller cells but not adjacent to any neurons. This is yet another structure that have not been previously described, yet is quite readily detected in the RC1 volume. We do not know the function of this organelle, its association with neurons known to use TRP-style channels is intriguing.

## *New Network Concepts: Sparseness and Joint Distributions*

Despite the very high density of connections in the retina, most occur largely as widely spaced singlets (very much like brain), especially in terms of amacrine cell inputs to ganglion cells. Understanding the relationships between neuronal sets requires knowing the full shape of the dendritic / axonal field and the patterning of synaptic inputs. The notion that one can summarize cell networks statistically is not supported by connectomics analysis of retinal connectivity. For example, there has been debate about whether retinal AII amacrine cells have

significant outflow to retinal ganglion cells (Kolb and Famiglietti 1975; Strettoi et al. 1992). In with both analyses (1) the scales of sampling are too small and (2) the assumption that sampling will be uniform across cells is wrong. Sampling is a joint distribution $J_{AB}$ of the physical intersections between two arbors $A_{XYZ}$ and $B_{XYZ}$ in 3D space: $J_{AB} = A_{XYZ} \cap B_{XYZ}$. Individual cell classes differ widely in neurite patterning (Reese 2008), so J will depend on the individual elements (Lauritzen et al. 2012). The axonal ribbons of ON cone bipolar cells are a perfect example. In a random instance of one ON bipolar cell class, the most likely outcome will be that no axonal ribbons will be observed. Does this not mean that axonal ribbons are some statistical fluke? Not at all. It means is that the distribution of targets that prefer ON bipolar cell input in the OFF sublayer is sparse, with a surfeit of axons but a deficit of targets. Importantly, every time a target encounters an ON bipolar cell axon, it does make a synapse. Thus the sampling by the target is perfect, but the statistics of the source appears variable. The latter is an illusion, the former is the result of joint distribution sampling. The same is true of the synapses of AII amacrine cells onto the dendrites of ganglion cells in the OFF layer (Anderson et al. 2011b). Again, sources far outnumber targets. AII ACs have large Hausdorff dimensions (they are highly space filling) and form far more output neurites than are required to completely target all the ganglion cells dendrites in the OFF volume. However, OFF alpha ganglion cell dendrites traversing the OFF layer receive input from every AII amacrine cell they encounter, again with perfect efficiency. This means that the classical practice of measuring output percentages from an afferent and computing synaptic variances has little meaning for network analysis.

# 4 Future Directions

## *4.1 Faster Connectome Builds*

Completeness is a new objective in neuroanatomy. Deciphering the individual motifs of brain and retinal networks requires the discovery all cell classes, all contacts and contact patterns. Every network we have explored shows new, unexpected motifs (Anderson et al. 2011b; Lauritzen et al. 2012; Marc et al. 2012), this goal is strongly justified. But the practice of high-resolution connectomics is not easily expanded. Our current build of mouse retina based on 1400 serial sections and large scale (0.28 mm diameter) is taking roughly 12 months. To do comparative studies of wiring differences across individuals, strains, species, etc., we need faster connectome builds (3-fold or more), especially if we are to explore large-scale neural reorganization in disease, development, and learning-memory transitions. No current platform is adequate. The simplest solution is building more platforms, of any type and running them continuously. ATEM systems have two advantages in that they can be repurposed from existing TEMs with appropriate software enhancements and all acquisition can be asynchronous. Unlike SBF SEM

or FIB SEM/STEM, a connectome acquisition on ATEM systems can be easily interspersed with other projects. Thus, ATEM systems are superb for core ultrastructural services. An ideal scheme for high-throughput connectomics would be a global build system (Fig. 13) that would require no new infrastructure. Existing arrays of TEM can be coordinated to image sets of grids for multiple projects and all data can be moved to cloud storage for project specific aggregation and queuing to distributed data-centers for connectome builds and database instantiation. Importantly, Viking is a web client with very low bandwidth demands, which means that annotation and analysis is fully open and distributed, and thousands of analysts can develop and refine connectomes simultaneously. We estimate that such a network of existing TEMs based on SerialEM acquisition, our new open source Nornir build system (available at GitHub), and Viking annotation, can accelerate connectome assembly and use by over 100-fold. In contrast, single system enhancements via faster cameras and more stable scanning stages may yield improvements 2-3x.

## *4.2 Improved molecular markers*

We need expanded libraries of molecular markers that are intrinsically compatible with electron imaging. Small molecule markers are ideal for ultrastructural imaging without compromising TEM contrast (Lauritzen et al. 2012; Marc et al. 2012; Jones et al. 2003; Marc and Liu 2000), but it is also important to exploit key macromolecules in connectivity mapping to differentiate synaptic partners suchas in array tomography (Micheva et al. 2010; Micheva and Bruchez 2011; Micheva and Smith 2007). So far, it has not been possible to merge the power of array tomography (which allows single-synapse molecular profiling) with electron imaging. There are two primary reasons for this. First, most antibodies against macromolecules were developed under conditions optimal for native or denatured protein detection, e.g. in Western blots, but not for highly epitopes found after TEM fixation. When such antibodies are found, they are happy accidents, but no more. A major advance would be the development of designed TEM-compliant antibodies. The second reason for limited use of protein markers is expression level: cell-class specific variations in total protein and variations in distribution. While the total amount of protein such as connexin 36 may be low, virtually all of it is located in transmembrane rafts of protein with approximate center-to-center spacing of 10 nm (Staehelin 1972), which corresponds to an effective concentration of 1-3 mM in epitope presentation. Another protein expressed at similar levels may be distributed uniformly throughout the cytoplasm of a cell with a mean nanomolar concentration: completely undetectable by conventional TEM immunocytochemistry.

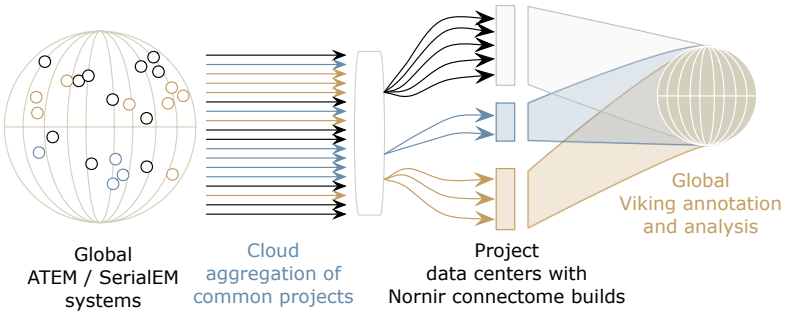


**Fig. 13** Massively scaling connectomics. Global collections of ATEM systems independently acquire large datasets for multiple projects. These are aggregated by cloud-based storage resources into common project datasets and distributed to data centers charged with their builds. All build become globally available via Viking-like web tools for annotation and analysis.

## *4.3 Neural Dynamics, Development and Disease*

A serious limitation of high-resolution connectomics is the inability to perform large scale statistical comparisons. While highly focused studies have enabled detailed descriptions of small-scale plasticity changes in neural architecture driven by different conditions, (Bourne and Harris 2011; Fiala et al. 2002; Sorra and Harris 2000), scaling up such efforts to analyze complete network variations in genetic and disease models is beyond current architectures. Early connectomics studies may help define canonical fields more precisely and support statistical studies on smaller volumes. For example, in advanced retinal degenerations, key neurons such as bipolar cells lose their dendrites and rewire in the inner plexiform layer (Jones et al. 2003; Jones et al. 2011), but the scope of that rewiring remains unknown. Rather than build an entire connectome containing over 100 rod bipolar cells (in 3-5 months), one could build and analyze 10 different connectomes of 10 rod bipolar cells each in the same time. But if one does not know the spatial domain of a target system, larger scale sampling will be critical and speeding up connectomics is a major objective.

## *Modeling*

What do we want to do with these complex network diagrams and lists of features? Clearly one goal is to generate rich models that allow parametric exploration of large scale systems (Hendrickson et al. 2012; Hay et al. 2011; Perin et al. 2013). The connectomics community will be responsible be exporting structural and network data in appropriate modeling formats such as variants of NEURON

(Hines and Carnevale 2001) and NeuroML (Gleeson et al. 2010). We are currently developing such tools using Python scripting and open access in the GitHub repository. One challenge is to exploit full 3D cell descriptors and spatial distributions of connections for modeling cells as non-compact entities. At present, Viking-based cellular elements are more richly defined than most modeling environments can accommodate, and modeling networks on multi-hop scales involving dozens of cells classes and thousands of copies demands advanced computational tools (Hendrickson et al. 2012)

**Acknowledgments** We thank the National Institutes of Health (EY02576, EY015128, and EY014800), National Science Foundation (0941717), the Thome Foundation, and Research to Prevent Blindness for support. We also thank Shoeb Mohammed for software development; and Hope Morrison, John Vo Hoang, and Noah Nelson for annotation.

References

Allen RA (1969) The retinal bipolar cells and their synapses in the inner plexiform layer. UCLA Forum Med Sci 8:101-143

Anderson JR, Grimm B, Mohammed S, Jones BW, Spaltenstein J, Koshevoy P, Tasdizen T, Whitaker R, Marc RE (2011a The Viking Viewer: Scalable multiuser annotation and summarization of large connectomics datasets. J Microscopy 241:13-28 doi:10.1111/j.1365-2818.2010.03402.x

Anderson JR, Jones B, Watt C, Shaw MV, Yang J-H, DeMill D, Lauritzen JS, Lin Y, Rapp KD, Mastronarde D, Koshevoy P, Grimm B, Tasdizen T, Whitaker R, Marc RE (2011b) Exploring the retinal connectome. Molecular Vision 17:355-379

Anderson JR, Jones BW, Yang J-H, Shaw MV, Watt CB, Koshevoy P, Spaltenstein J, Jurrus E, UV K, Whitaker R, Mastronarde D, Tasdizen T, Marc RE (2009) A computational framework for ultrastructural mapping of neural circuitry. PLoS Biol 7 (3):e1000074

Aster R, Borchers B, Thurber C (2005) Parameter Estimation and Inverse Problems. Academic Press, NY

Barabási A-L, Albert R (1999) Emergence of scaling in random networks. Science 286:509–512

Barmpoutis D, Murray RM (2010) Networks with the smallest average distance and the largest average clustering. arXiv 1007.4031

Barthelemy M, Amaral LAN (1999) Small-world networks: Evidence for a crossover picture. Phys Rev Lett 82:3180-3183

Bennett CL, Larson D, Weiland JL, Jarosik N, Hinshaw G, Odegard O, Smith KM, Hill RS, Gold B, Halpern M, Komatsu E, Nolta MR, Page L, Spergel DN, Wollack E, Dunkley J, Kogut A, Limon M, Meyer SS, Tucker GS, Wright EL (2013) Nine-year Wilkinson Microwave Anisotropy Probe (WMAP) observations: Final maps and results. arXiv 1212.5225v3 [astro-ph.CO]

Benson DL, Huntley GW (2012) Building and remodeling synapses. Hippocampus 22:954–968

Boergens KM, Denk W (2013) Controlling FIB-SBEM slice thickness by monitoring the transmitted ion beam. J Microsc 252:258-262

Bollobás B (1998) Modern Graph Theory. Springer, New York

Bourne JN, Harris KM (2011) Nanoscale analysis of structural synaptic plasticity. Current Opinion in Neurobiology 22:1-11. doi:10.1016/j.conb.2011.10.019

Briggman KL, Denk W (2006) Towards neural circuit reconstruction with volume electron microscopy techniques. Current Opinion in Neurobiology 16:562-570

Briggman KL, Helmstaedter M, Denk W (2011) Wiring specificity in the direction-selectivity circuit of the retina. Nature 471:138-188

Brill MH (1990) Mesopic color matching: some theoretical issues. J Opt Soc Am A 7:2048-2051

Buck SL (1997) Influence of rod signals on hue perception: evidence from successive scotopic contrast. Vision Res 37:1295-3101

Buck SL (2004) Rod-cone interactions in human vision. In: Chalupa LM, Werner J (eds) Visual Neurosciences, vol 1. MIT Press, Cambridge, MA, pp 863-878

Buck SL, Stefurak DL, Moss C, Regal D (1984) The time-course of rod-cone interaction. Vision Res 24:543-548

Chua J, Nivison-Smith L, Tan SS, Kalloniatis M (2013) Metabolic profiling of the mouse retina using amino acid signatures: Insight into developmental cell dispersion patterns. Experimental Neurology 250:74-93

Cohen AI (1965) Some electron microscopic observations on inter-receptor contacts in the human and macaque retinae. J Anat 99:595–610

Cover TM, Hart PE (1967) Nearest neighbor pattern classification. IEEE Transactions on Information Theory IT-13:21-27

Deisseroth K (2011) Optogenetics. Nat Methods 8:26-29

Diestel R (2005) Graph Theory. 3rd edn. Springer-Verlag, Heidelberg

Dumitrescu ON, Pucci FG, Wong KY, Berson DM (2009) Ectopic retinal ON bipolar cell synapses in the OFF inner plexiform layer: Contacts with dopaminergic amacrine cells and melanopsin ganglion cells. Journal Comp Neurol 517:226-244

Famiglietti EVJ, Kolb H (1975) A bistratified amacrine cell and synaptic circuitry in the inner plexiform layer of the retina. Brain Res 84:293-300

Fiala JC (2005) Reconstruct: a free editor for serial section microscopy. J Microsc 218:52-61

Fiala JC, Spacek J, Harris KM (2002) Dendritic spine pathology: cause or consequence of neurological disorders? Brain Research Reviews 39:29-54

Frumkes TE, Eysteinsson T (1988) The cellular basis for suppressive rod-cone interaction. Vis Neurosci 1:263-273

Gleeson P, Crook S, Cannon RC, Hines ML, Billings GO, Farinella M, Morse TM, Davison AP, Ray S, Bhalla US, Barnes SR, Dimitrova YD, Silver RA (2010) NeuroML: A language for describing data driven models of neurons and networks with a high degree of biological detail. PLoS Comp Biol 6:e1000815

Goldberg SH, Frumkes TE, Nygaard RW (1983) Inhibitory influence of unstimulated rods in the human retina: evidence provided by examining cone flicker. Science 221:180-182

Google (2010) KML Reference – KML – Google Code. Google, Inc.,

Han Y, Massey S (2005) Electrical synapses in retinal ON cone bipolar cells: subtype-specific expression of connexins. Proc Natl Acad Sci U S A 102:13313-13318

Harary F, Palmer EM (1973) Graphical Enumeration. Academic Press, New York

Hay E, Hill S, Schürmann F, Markram H, Segev I (2011) Models of eocortical Lalyer 5b pyramidal cells capturing a wide range of dendritic and perisomatic active properties. PLoS Comput Biol 7:e1002107

Helmstaedter M, Briggman KL, Denk W (2008) 3D structural imaging of the brain with photons and electrons. Curr Opin Neurobiol 18:633-641

Helmstaedter M, Briggman KL, Turaga SC, Jain V, Seung HS, Denk W (2013) Connectomic reconstruction of the inner plexiform layer in the mouse retina. Nature 500:168-174

Hendrickson PJ, Yu GJ, Robinson BS, Song D, Berger TW (2012) Towards a large-scale biologically realistic model of the hippocampus. Conf Proc IEEE Eng Med Biol Soc 2012:4595-4598

Hines ML, Carnevale NT (2001) NEURON: a tool for neuroscientists. The Neuroscientist 7:123-135

Hoshi H, Liu W-L, Massey SC, Mills SL (2009) ON inputs to the OFF layer: Bipolar cells that break the stratification rules of the retina. J Neurosci 29:8875-8883. doi:10.1523/jneurosci.0912-09.2009

Hueser J (2000) How to convert a traditional electron microscopy laboratory to digital imaging: Follow the 'Middle Road'. Traffic 1:614–621

Jagadeesh V, Manjunath BS, Anderson JR, Jones BW, Marc RE, Fisher SK (2013) Robust segmentation based tracing using an adaptive wrapper for inducing priors. IEEE Trans Image Process 22:4952-2063

Jeong W, Beyer J, Hadwiger M, Blue R, Law C, Vazquez A, Reid C, Lichtman J, Pfister H (2010) SSECRETT and NeuroTrace: Interactive Visualization and Analysis Tools for Large-Scale Neuroscience Datasets. IEEE Computer Graphics and Applications 30:58-70

Jones BW, Kondo M, Terasaki H, Watt CB, Rapp K, Anderson JR, Lin Y, Shaw MV, Yang JH, Marc RE (2011) Retinal remodeling in the Tg P347L rabbit, a large-eye model of retinal degeneration. J Comp Neurol 519:2713-2733

Jones BW, Watt CB, Frederick JM, Baehr W, Chen CK, Levine EM, Milam AH, LaVail MM, Marc RE (2003) Retinal remodeling triggered by photoreceptor degenerations. J Comp Neurol 464:1-16

Kalloniatis M, Marc RE, Murry RF (1996) Amino acid signatures in the primate retina. J Neurosci 16:6807-6829

Karp RM (1972) Reducibility Among Combinatorial Problems. In: Miller RE, Thatcher JW (eds) Complexity of Computer Computations. Plenum, New York, pp 85–103

Kleinfeld D, Bharioke A, Blinder P, Bock DD, Briggman KL, Chklovskii DB, Denk W, Helmstaedter M, Kaufhold JP, Lee WC, Meyer HS, Micheva KD, Oberlaender M, Prohaska S, Reid RC, Smith SJ, Takemura S, Tsai PS, Sakmann B (2011) Large-Scale Automated Histology in the Pursuit of Connectomes. J Neurosci 31:16125-16138

Knott G, Marchman H, Wall D, Lich B (2008) Serial section scanning electron microscopy of adult brain tissue using focused ion beam milling. J Neurosci 28:2959-2964

Kolb H (1977) The organization of the outer plexiform layer in the retina of the cat: electron microscopic observations. J Neurocytol 6:131-153

Kolb H, Famiglietti EV (1974a) Rod and cone pathways in the inner plexiform layer of cat retina. Science 186:47-49

Kolb H, Famiglietti EVJ (1974b) Rod and cone pathways in the retina of the cat. Invest Ophthal 15:935-946

Lange G, Denny N, Frumkes TE (1997) Suppressive rod-cone interactions: evidence for separate retinal (temporal) and extraretinal (spatial) mechanisms in achromatic vision. J Opt Soc Am A Opt Image Sci Vis 14:2487-2498

Lauritzen JS, Anderson JR, Jones BW, Watt CB, Mohammed S, Hoang JV, Marc RE (2012) ON cone bipolar cell axonal synapses in the OFF inner plexiform layer of the rabbit retina. J Comp Neurol 521:977-1000

Lauritzen JS, Hoang JV, Sigulinsky C, Jones BW, Anderson JR, Watt CB, Mohammed S, Marc RE (2013) Tiered cross-class bipolar cell gap junctional coupling in the rabbit retina. Invest Ophthal 54:1754

Lee SC, Cowgill EJ, Al-Nabulsi A, Quinn EJ, Evans SM, Reese BE (2011) Homotypic regulation of neuronal morphology and connectivity in the mouse retina. J Neurosci 31:14126-14133

Li X, Kamasawa N, Ciolofan C, Olson CO, Lu S, Davidson KGV, Yasumura T, Shigemoto R, Rash JE, Nagy JI (2008) Connexin45-containing neuronal gap junctions in rodent retina also contain connexin36 in both apposing hemiplaques, forming bi-homotypic gap junctions, with scaffolding contributed by zonula occludens-1. J Neurosci 28:9769–9789

Lynn BD, Li X, Nagy JI (2012) Under construction: Building the macromolecular superstructure and signaling components of an electrical synapse. J Membr Biol 245:303–317

MacNeil MA, Heussy JK, Dacheux RF, Raviola E, Masland RH (1999) The shapes and numbers of amacrine cells: Matching of photofilled with Golgi-stained cells in the rabbit retina and comparison with other mammalian species. J Comp Neurol 413:305-326

MacNeil MA, Heussy JK, Dacheux RF, Raviola E, Masland RH (2004) The population of bipolar cells in the rabbit retina. J Comp Neurol 472:73-86

MacQueen J (1967) Some methods for classification and analysis of multivariate observations. In: Proc. 5th Berkeley Symposium. pp 281–297

Marc RE (2010) Synaptic Organization of the Retina. In: Levin LA, Nilsson SFE, Ver Hoeve J, Wu SM, Kaufman PL, Alm A (eds) Adler's Physiology of the Eye. Elsevier, pp 443-458

Marc RE, Anderson JR, Jones BW, Watt CB, Lauritzen JS (2013) Retinal Connectomics: Towards complete, accurate networks. Prog Retin Eye Res 37:141-162

Marc RE, Cameron DA (2001) A molecular phenotype atlas of the zebrafish retina. Journal of Neurocytology 30:593-654

Marc RE, Jones BW (2002) Molecular phenotyping of retinal ganglion cells. J Neurosci 22:412-427

Marc RE, Jones BW, Lauritzen JS, Watt CB, Anderson JR (2012) Building Retinal Connectomes. Current Opinion in Neurobiology 22:568-574

Marc RE, Liu W (2000) Fundamental GABAergic amacrine cell circuitries in the retina: nested feedback, concatenated inhibition, and axosomatic synapses. J Comp Neurol 425 (4):560-582

Marc RE, Liu WL, Kalloniatis M, Raiguel SF, van Haesendonck E (1990) Patterns of glutamate immunoreactivity in the goldfish retina. J Neurosci 10 (12):4006-4034

Marc RE, Liu WL, Muller JF (1988) Gap junctions in the inner plexiform layer of the goldfish retina. Vision Research 28 (1):9-24

Marc RE, Murry RF, Basinger SF (1995) Pattern recognition of amino acid signatures in retinal neurons. J Neurosci 15 (7 Pt 2):5106-5129

Marc RE, Murry RF, Fisher SK, Linberg KA, Lewis GP, Kalloniatis M (1998) Amino acid signatures in the normal cat retina. Investigative Ophthalmology & Visual Science 39 (9):1685-1693

Mastronarde DN (2005) Automated electron microscope tomography using robust prediction of specimen movements. J Struct Biol 152:36-51

Micheva KD, Bruchez MP (2011) The gain in brain: novel imaging techniques and multiplexed proteomic imaging of brain tissue ultrastructure. Current Opinion in Neurobiology. doi:10.1016/j.conb.2011.08.004

Micheva KD, Busse B, Weiler NC, O'Rourke N, Smith SJ (2010) Single-synapse analysis of a diverse synapse population: proteomic imaging methods and markers. Neuron 68:639-653

Micheva KD, Smith SJ (2007) Array tomography: A new tool for imaging the molecular architecture and ultrastructure of neural circuits. Neuron 55:25-36

Mikula S, Trotts I, Stone JM, Jones EG (2007) Internet-enabled high-resolution brain mapping and virtual microscopy. Neuroimage 35 (1):9-15. doi:S1053-8119(06)01176-1 [pii]
10.1016/j.neuroimage.2006.11.053

Mizoguchi A, Nakanishi H, Kimura K, Matsubara K, Ozaki-Kuroda K, Katata T, Honda T, Kiyohara Y, Heo K, Higashi M, Tsutsumi T, Sonoda S, Ide C, Takai Y (2002) Nectin: an adhesion molecule involved in formation of synapses. J Cell Biol 156:555–565

Morales J, Rodríguez A, Rodríguez JR, Defelipe J, Merchán-Pérez A (2013) Characterization and extraction of the synaptic apposition surface for synaptic geometry analysis. Front Neuroanat 7:20. doi:10.3389/fnana.2013.00020

Morgan JL, Lichtman JW (2013) Why not connectomics. Nature Methods 10:494-500

Ogita H, Ritake Y, Miyoshi J, Takai Y (2010) Cell adhesion molecules nectins and associating proteins: Implications for physiology and pathology. Proc Jpn Acad 86:621-629

Perin R, Telefont M, Markram H (2013) Computing the size and number of neuronal clusters in local circuits. Front Neuroanat 7:1-10

Prinz AA, Bucher B, Marder E (2004) Similar network activity from disparate circuit parameters. Nature Neuroscience 7:1345-1352

Raviola E, Gilula NB (1975) Intramembrane organization of specialized contacts in the outer plexiform layer of the retina. A freeze-fracture study in monkeys and rabbits. J Cell Biol 65:192-222

Reese BE (2008) Mosaics, Tiling and Coverage by Retinal Neurons. In: Masland RH, Albright T (eds) The Senses, vol Volume 1. Academic Press, San Diego, pp 439-456

Rockhill RL, Daly FJ, MacNeil MA, Brown SP, Masland RH (2002) The Diversity of Ganglion Cells in a Mammalian Retina. J Neurosci 22(3831–3843

Sorra KE, Harris KM (2000) Overview on the structure, composition, function, development, and plasticity of hippocampal dendritic spines. Hippocampus 10:501-511

Stabell B, Stabell U (1998) Chromatic rod-cone interaction during dark adaptation. J Opt Soc Am A Opt Image Sci Vis 15:2809-2815

Stabell B, Stabell U (2002) Effects of rod activity on color perception with light adaptation. J Opt Soc Am A Opt Image Sci Vis 19:1249-1258

Staehelin LA (1972) Three types of gap junctions interconnecting intestinal epithelial cells visualized by freeze-etching. Proc Natl Acad Sci U S A 69:1318–1321

Stevens JK, Davis TL, Friedman N, Sterling P (1980) A systematic approach to reconstructing microcircuitry by electron microscopy of serial sections. Brain Res 2: 265-293

Strettoi E, Dacheux RF, Raviola E (1990) Synaptic connections of rod bipolar cells in the inner plexiform layer of the rabbit retina. J Comp Neurol 295:449-466

Strettoi E, Raviola E, Dacheux RF (1992) Synaptic connections of the narrow-field, bistratified rod amacrine cell (AII) in the rabbit retina. J Comp Neurol 325:152-168

Tasdizen T, Koshevoy P, Grimm B, Anderson JR, Jones BW, Whitaker R, Marc RE (2010) Automatic mosaicking and volume assembly for high-throughput serial-section transmission electron microscopy J Neuroscience Methods 193:132-144

Thomas LP, Buck SL (2006) Foveal and extra-foveal influences on rod hue biases. Vis Neurosci 23:539-542

Trezona PW (1970) Rod participation in the 'blue' mechanism and its effect on colour matching. Vision Res 10:317-332

Trezona PW (1973) The tetrachromatic colour match as a colorimetric technique. Vision Res 13:9-25

van den Heuvel MP, Sporns O (2011) Rich-club organization of the human connectome. J Neurosci 31 (44):15775-15786. doi:10.1523/jneurosci.3539-11.2011

Van Essen DC, Glasser MF, Dierker DL, Harwell J, Coalson T (2011) Parcellations and Hemispheric Asymmetries of Human Cerebral Cortex Analyzed on Surface-Based Atlases. Cerebral Cortex 22:2241-2262 doi:10.1093/cercor/bhr291

Watts DJ, Strogatz SH (1998) Collective dynamics of ‘small- world’ networks. Nature 393:440-442

Wong E, Baur B, Quader S, Huang C-H (2012) Biological network motif detection: principles and practice. Brief Bioinform 13:202-215 doi:10.1093/bib/bbr033

Xie X, Schnieder MC, Sánchez-Sinencio E, Embabi SHK (1999) Sound design of low power nested transconductance-capacitance compensation amplifiers. IEEE Electronics Letters 35:956–958